RESEARCH ARTICLE

A leader-return-stroke consistent macroscopic model for calculations of return stroke current and its optical and electromagnetic emissions

Shuyao Cai[1], Mingli Chen[1] (ID), Yaping Du[1], and Zilong Qin[1] (ID)

[1]Department of Building Services Engineering, The Hong Kong Polytechnic University, Kowloon, Hong Kong

Abstract A downward lightning flash usually starts with a downward leader and an upward connecting leader followed by an upward return stroke. It is the preceding leader that governs the following return stroke property. Besides, the return stroke property evolves with height and time. These two aspects, however, are not well addressed in most existing return stroke models. In this paper, we present a leader-return stroke consistent model based on the time domain electric field integral equation, which is a growth and modification of Kumar's macroscopic model. The model is further extended to simulate the optical and electromagnetic emissions of a return stroke by introducing a set of equations relating the return stroke current and conductance to the optical and electromagnetic emissions. With a presumed leader initiation potential, the model can then simulate the temporal and spatial evolution of the current, charge transfer, channel size, and conductance of the return stroke, furthermore the optical and electromagnetic emissions. The model is tested with different leader initiation potentials ranging from -10 to -140 MV, resulting in different return stroke current peaks ranging from 2.6 to 209 kA with different return stroke speed peaks ranging from 0.2 to 0.8 speed of light and different optical power peaks ranging from 4.76 to 248 MW/m. The larger of the leader initiation potential, the larger of the return stroke current and speed. Both the return stroke current and speed attenuate exponentially as it propagates upward. All these results are qualitatively consistent with those reported in the literature.

1. Introduction

The negative cloud-to-ground ($-$CG) flash is the most studied lightning event, owing to both the fact that it produces most of the damage attributable to lightning and the fact that it produces the most measurable optical and electromagnetic signature. A downward $-$CG usually starts with a downward negatively charged leader, followed by an upward positively charged return stroke. It may consist 1 to 27 more leader/return stroke processes, with the peak current of the return stroke ranging from the minimum 2 kA to the maximum 200 kA and an action integral ranging from 0.5 to 500 kA^2s and an instantaneous power up to 10^{11} W [*Rakov and Uman*, 2003]. The power gives out in heat and electromagnetic energies, causing damages to lives and facilities on Earth.

Research of the return stroke can be tracked back to 1750s when Benjamin Franklin invented the lightning rod. The first observation of the return stroke current was achieved by *McCann* [1944] in USA with shunts installed on tall towers. After that, measurements of the return stroke currents on tall towers were also made in Switzerland [*Berger*, 1975], Germany [*Fuchs et al.*, 1998], and Brazil [*Pinto et al.*, 2005]. *Lin et al.* [1980] summarized the properties of typical vertical electric and horizontal magnetic fields of return strokes measured on ground in the distance of 1–200 km. Optical observations of return strokes included photograph taking, light intensity, and spectral measurements. The return stroke speed read from photographs taken by the steak camera was in the range of one third to two thirds speed of the light [*Idone and Orville*, 1982]. Some researchers argued that the return stroke speed obtained from the light signal could not be the same to that of the current propagation [*Zhou et al.*, 2014]. *Guo and Krider* [1982] evaluated the peak value of light power of the return stroke in the distance of 5–35 km based on the measurement of optical signals in the wavelength band of 400–1100 nm.

Numerical modeling of the return stroke can be classified into four types [*Rakov and Uman*, 1998] or a combination of the 4. The first one is the gas dynamic model, which studies the radial evolution of short lightning channel segment, showing the change of mass, momentum, and energy, hence the temperature and
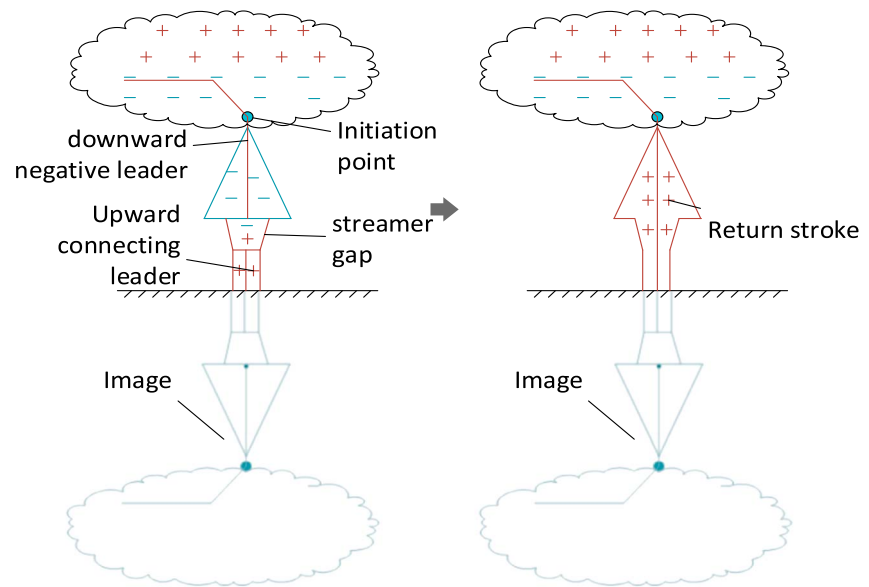
Figure 1. Illustration of formation of leader-return stroke channel.

pressure, based on the gas dynamic equations [*Plooster*, 1970, 1971]. The second one is the electromagnetic model, which treats the return stroke channel as a lossy electromagnetic antenna [*Podgorski and Landt*, 1987; *Moini et al.*, 1997]. The third one is the distributed-circuit model, which treats the return stroke channel as a transmission line with certain values of resistance, inductance, and capacitance [*Gorin and Markin*, 1975; *Baum and Baker*, 1990; *Chen and Du*, 2009; *Du and Chen*, 2010; *Du et al.*, 2012]. The fourth one is the engineering model, which relates the return stroke current with height and time based on experimental data and empirical math formulas [*Rakov*, 1997].

Recent years, *Kumar et al.* [2008] proposed a macroscopic model for the return stroke, which treats the lightning channel as a long arcing discharge and describes the current and electric fields in the channel with the electromagnetic field integral equations (time domain electric field integral equation (TD-EFIE)) [*Raysaha et al.*, 2011, 2012; *Kumar and Raysaha*, 2013]. Given the channel initial condition, the model can simulate the spatial and temporal evolution of the current, charge transfer, and conductance along the return stroke channel. In this study, we present a leader-return-stroke coupled macroscopic model, which is a growth and extension of Kumar's model with modifications made at several aspects. The model includes two parts: modeling of the return stroke channel (section 2) and that of the light and electromagnetic emission of the return stroke (section 3). The modeling results and discussions of the results are presented in section 4.

2. Modeling of Return Stroke Channel

2.1. Return Stroke Channel Formation

As shown in Figure 1, a thundercloud usually has a typical three charge layer structure. A $-$CG usually starts with a leader process initiated at the lower part of the thundercloud. Subjected to the electric potential profile in and out the thundercloud, the leader usually extends from the initiation point in both upward and downward directions. This is well known as the bidirectional leader concept for interpretation of a variety of lightning physical process [*Mazur and Ruhnke*, 1998; *Riousset et al.*, 2007; *Chen et al.*, 2013]. The downward part is negatively charged and propagates to ground, while the upward part is positively charged with branches stretching into the upper part of the thundercloud.

The channel of the downward leader part consists of a thin conductive core surrounded by a corona sheath. As the downward negative leader (DNL) approaches the ground, the electric field on ground increases. When the ground electric field is enhanced to the critical electrical field for positive breakdown (E_{C+}), first, a positive streamer and then a positive upward connecting leader (UCL) appear there. As the UCL and DNL approach to each other, the electric field in the gap between them increases rapidly. When the electric field in the gap
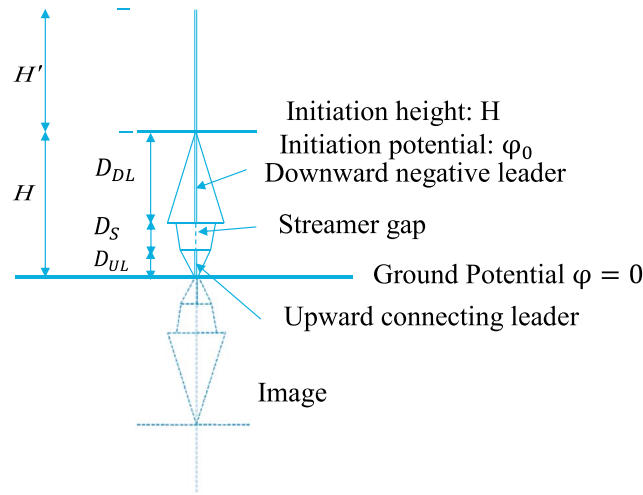
Figure 2. Illustration of modeling of leader-return stroke channel.

between the DNL and UCL reaches the critical electric field for negative breakdown (E_C), i.e., the negative streamer zone in front of the DNL touches the UCL head, a final breakdown occurs, and hence, a return stroke process is initiated. The return stroke usually starts with two current waves generated at the UCL and DNL connecting point, one moving upward and the other moving downward [*Wang et al.*, 2014; *Raysaha et al.*, 2012]. The downward wave reflects at the ground and propagates upward to catch up the previous upward wave. As the return stroke current wave propagates upward, the preexisting leader channel is ionized further, resulting in further changes of channel radius, temperature, and conductivity. The property of the return stroke basically depends on the preceding leader channel.

2.2. Initial Condition of Return Stroke Channel

The condition of the preceding leader channel just before the return stroke can be taken as the initial condition of the return stroke. As shown in Figure 2, the leader channel is assumed to originate at an initiation height H with an initiation potential φ_0 and extend bidirectionally. The downward portion below the initiation height is measured H, and the upward portion above the initiation height is measured H'. For the downward portion, it includes a DNL channel (D_{DL}), a UCL channel (D_{UL}), and a streamer gap (Ds). The ground is conductive, and its potential is set to zero. Both the DNL and UCL channel are consisted of a thin inner core surrounded by a corona sheath. The radius of the leader core (r_0) is usually in the range of 1–5 mm and that of corona sheath may be in the range of several to tens of meters. The channel core is expected to expand after the return stroke onset and reach a few centimeters in radius [*Rakov*, 1998].

The late stage DNL parameters, as the initial parameters of the return stroke, are based on the leader propagation model of *Xu and Chen* [2013]. Based on that model, the leader channel line charge density λ_L (z) (negative polarity) and corona sheath radius r_S (z) in relation to the leader initiation height (H) and root potential φ_0 (negative polarity) can be simplified as

$$\lambda_L(Z) = a\lambda_0 \exp(-b \cdot z) + \lambda_0(1-a)(1-z/H), \tag{1}$$

$$r_S(Z) = \lambda_L(Z)/[2\pi\varepsilon_0 E_C(Z)], \tag{2}$$

$$\lambda_0 = 0.0226\varphi_0^{0.859}, \tag{3}$$

where λ_0 is the leader tip charge density at its last stage just before the attachment, a is a constant of about 0.6, and b is a constant of about 7×10^{-3} m^{-1} for $H < 5000$ m and about 5×10^{-3} m^{-1} for $H \geq 5000$ m. $E_C(z)$ is the critical electric field for negative breakdown, which is a function of the altitude above ground as $E_C = E_{C0}e^{-z/8400}$.

The length from the DNL tip to the ground when the UCL appears (Ds_+) and the length of the streamer gap (Ds) between DNL and UCL, which is similar to the striking distance, can be estimated as

$$Ds_+ = -\varphi_{tip}/E_{C0+}, \quad Ds = \varphi_{tip}/E_{C0}, \tag{4}$$

where φ_{tip} is the DNL leader tip potential right before the return stroke and E_{C0+} (about +500 kV/m) and E_{C0} (about −750 kV/m) are the critical electrical field at ground level for positive and negative polarities, respectively. Assume that the UCL and DNL have the same speed just before the return stroke, the length of UCL can then be estimated as $D_{\text{UL}} = (Ds_+ - Ds)/2$.

The DNL current (I_{DL}) right before the return stroke is based on the model results of *Xu and Chen* [2013] as

$$I_{\text{DL}} = 0.1314\varphi_0^{1.502}. \tag{5}$$

The UCL current (I_{UL}) right before the return stroke is assumed to be a fraction of that of the DNL, say $0.3I_{\text{DL}}$. The streamer gap current (I_{ST}) right before the return stroke varies from I_{DL} when around the DNL tip down to I_{UL} when around the UCL tip.

Although the leader electric field value varies significantly over time [*Popov*, 2003], the value just before the return stroke is concerned. The longitudinal electrical field in both DNL and UCL channels just before the return stroke can be related to their leader current as

$$E_{\text{DL}} = C_b/I_{\text{DL}}, \qquad E_{\text{UL}} = C_b/I_{\text{UL}}, \tag{6}$$

where C_b is a constant of about 30,000 W/m based on lab experiments [*Raizer*, 1991].

The DNL tip potential is estimated as

$$\varphi_{\text{tip}} = \varphi_0 - E_{\text{DL}}(H - Ds - D_{\text{UL}}). \tag{7}$$

The equivalent channel resistance per unit length of the DNL channel (Z_{DL}), the UCL channel (Z_{UL}), and the streamer gap channel (Z_{ST}), as the initial values of the return stroke channel, are estimated as

$$Z_{\text{DL}} = E_{\text{DL}}/I_{\text{DL}}, Z_{\text{UL}} = E_{\text{UL}}/I_{\text{UL}}, \text{ and } Z_{\text{ST}} = E_{C0}/I_{\text{ST}}. \tag{8}$$

2.3. Modeling of Return Stroke Current

The return stroke is supposed to start when UCL and DNL accelerate within the streamer gap, producing a transient current pulse that propagates bidirectionally (downward and upward from the connection point) along the channel [*Tran and Rakov*, 2015]. As the downward one reaches the ground, it reflects and moves upward to catch up the previous upward one. The current propagation behavior is subjected to the total longitudinal electrical field in the channel core including the scattered field and the field due to cloud and leader charges. A time domain electric field integral equation (TD-EFIE) for solving vertical thin-wire structure electromagnetic problems derived by *Miller et al.* [1973] is

$$\hat{z} \cdot \overrightarrow{E}^A(\hat{z},t) - \frac{\mu_0}{4\pi} \int_{c\left(\overrightarrow{z}\right)} \begin{bmatrix} \dfrac{\hat{z} \cdot \hat{z'}}{R} \dfrac{\partial}{\partial t'} I(z',t') \\[2mm] +c\dfrac{\hat{z} \cdot \overrightarrow{R}}{R^2} \dfrac{\partial}{\partial z'} I(z',t') \\[2mm] -c^2 \dfrac{\hat{z} \cdot \overrightarrow{R}}{R^3} \lambda(z',t') \end{bmatrix} dz' = I(z,t)Z(z,t) \tag{9}$$

The accumulated line charge density (positive polarity) in the channel during the return stroke can be evaluated based on the continuity equation:

$$\frac{\partial}{\partial z'}I(z',t') = -\frac{\partial}{\partial t'}\lambda(z',t') \tag{10}$$

where μ_0 is the permeability, ε_0 is the permittivity of free space, I is the current, and Z is the channel resistance per meter. The z represents the channel element under consideration and z' the any element along the

channel. The $\hat{z}$ is the unit vector for z. The $\overrightarrow{E}^A$ is the initial longitudinal electric field in the channel, which depends on the cloud and leader sheath charge just before the return stroke:

$$E^A(z) = \begin{cases} E_{DL} & z \in D_{DL} + H' \\ E_{ST} & z \in D_S \\ E_{UL} & z \in D_{UL} \end{cases} \tag{11}$$

The integral term in equation (9) is known as the scattered field, which is represented with E^B hereafter. $\overrightarrow{R}$ is the vector distance pointing from z' to z, and $t' = t\text{-}R/c$ is the time delay from z' to z. The $C(\overrightarrow{z})$ represents the whole channel $H + H'$ and its mirror image on ground.

Since the return stroke front is propagating along the previously existing leader channel that is a thin conductive core surrounded by a thick corona sheath with negative charges, parts of the positive charges accumulated on the core by the return stroke current front will diffuse into the corona sheath to neutralize the negative charges there. The positive charge diffusing rate depends on the product of the corona sheath conductivity and radial electric field produced by the positive charges on the core surface. Assume that the line density of positive charges on the core is λ_C (z', t') and that diffused into the corona sheath is λ_S (z', t'), the radial electric field on the core surface will be λ_C $(z', t')/\varepsilon_0$. If we assign the corona sheath a uniform line conductivity of σ_S, which is taken as 10 μS/m in this study [*Maslowski and Rakov, 2006*], then we have

$$\lambda(z', t') = \lambda_C(z', t') + \lambda_S(z', t'), \tag{12}$$

$$\frac{\partial}{\partial t'}\lambda_C(z', t') = -\frac{\partial}{\partial t'}\lambda_S(z', t') = -\frac{\sigma_S}{\varepsilon_0}\lambda_C(z', t'), \tag{13}$$

$$r_S(z', t') = [\lambda_L(z') + \lambda_S(z', t')]/[2\pi\varepsilon_0 E_C(z')]. \tag{14}$$

where r_S (z', t') represents the changing corona sheath radius derived from equation (2), and for $z' > H$ it is supposed to be no larger than r_S (H, t').

2.4. Computing Scheme for the Model
2.4.1. Numerical Solution for the Current
The channel $H + H' \approx 2H$ is divided into $2N$ number of very small spatial element each with a length of Δs. The evolution time is divided into M number of time step each with an interval of Δt. To achieve good accuracy and adapt to the speed of light c, the spatial element size Δs is related to the time step Δt by $\Delta s = 2c\Delta t$. From equation (10), taking the current in element i at time step j as $I_{i,j}$, the line density of charges accumulated in element i at step j is given by

$$\lambda_{i,j} = \lambda_{i,j-1} + \frac{\Delta t}{2\Delta s}\left(I_{i-1,j-1} - I_{i+1,j-1}\right) \tag{15}$$

Similarly, from equations (11)–(13), the numerical solutions for λ_C (z', t'), λ_S (z', t') and r_S (z', t') for element i at time j are given by

$$\lambda_{C,i,j} = \lambda_{C,i,j-1} \cdot e^{-\frac{\sigma_S}{\varepsilon_0}\Delta t} + \frac{\Delta t}{2\Delta s}\left(I_{i-1,j-1} - I_{i+1,j-1}\right). \tag{16}$$

$$\lambda_{S,i,j} = \lambda_{S,i,j-1} + \lambda_{C,i,j-1} \cdot \left(1 - e^{-\frac{\sigma_S}{\varepsilon_0}\Delta t}\right). \tag{17}$$

$$r_{S,i,j} = r_{S,i,0} + \lambda_{S,i,j}/\left(2\pi\varepsilon_0 E_{C,i}\right). \tag{18}$$

where $\lambda_{i,0} = \lambda_{C,i,0} = \lambda_{S,i,0} = 0$, and $r_{S,i,j} = r_{S,N,j}$, for $i > N$.

In such, the TD-EFIE equation can be rewritten as

$$E_i^A - E_{i,j}^B = I_{i,j}Z_{i,j} \tag{19}$$

Set $N_{UL} = D_{UL}/\Delta s$, $N_{ST} = Ds/\Delta s$, and $2N = (H + H')/\Delta s$, then

$$E_i^A = \begin{cases} E_{DL} & \text{for } i = N_{UL} + N_{ST} \sim 2N \\ E_{ST} & \text{for } i = N_{UL} \sim N_{UL} + N_{ST} \\ E_{UL} & \text{for } i = 1 \sim N_{UL} \end{cases} \tag{20}$$

Taking account of the space integral effect of each element Δs, the integral convergence as well as the charge diffusing effect, $E_{i,j}^B$ can then be written as

$$E_{i,j}^B = E_{i,j} + \frac{\mu_0}{4\pi} \sum_{\substack{u = u' = 1 \\ u \neq i}}^{2N} \left[\begin{array}{c} \frac{I_{u,v} - I_{u,v-1}}{\Delta t} \cdot \ln\left(\frac{|u-i|+0.5}{|u-i|-0.5}\right) \\[2mm] + \frac{I_{u',v'} - I_{u',v'-1}}{\Delta t} \cdot \ln\left(\frac{u'+i-0.5}{u'+i-1.5}\right) \\[2mm] + \frac{I_{u+1,v} - I_{u-1,v}}{2\Delta s} \cdot \frac{i-u-0.5}{|i-u-0.5|} \cdot c \cdot \ln\left(\frac{|u-i|+0.5}{|u-i|-0.5}\right) \\[2mm] + \frac{I_{u'+1,v'} - I_{u'-1,v'}}{2\Delta s} \cdot c \cdot \ln\left(\frac{u'+i-0.5}{u'+i-1.5}\right) \\[2mm] - \frac{\lambda_{C,u,v} + \alpha_{u,v}\lambda_{S,u,w}}{\Delta s} \cdot \frac{i-u}{|i-u|} \cdot c^2 \cdot \frac{1}{(u-i)^2 - 0.25} \\[2mm] + \frac{\lambda_{C,u',v'} + \alpha_{u',v'}\lambda_{S,u',w'}}{\Delta s} \cdot c^2 \cdot \frac{1}{(u'+i-1)^2 - 0.25} \end{array} \right] = E_{i,j} + E_{i,j}^C \tag{21}$$

where

$$v = j - 2|u-i|, \quad w = j - \text{int}\left(\frac{2|u-i|}{\alpha_{u,v}}\right),$$

$$v' = j - 2(i+u'-1), \quad w' = j - \text{int}\left(\frac{2(i+u'-1)}{\alpha_{u',v'}}\right),$$

$$\alpha_{u,v} = \frac{|u-i|}{\sqrt{(u-i)^2 + (r_{S,u,v}/\Delta s)^2}}, \quad \alpha_{u',v'} = \frac{|u'+i-1|}{\sqrt{(u'+i-1)^2 + (r_{S,u',v'}/\Delta s)^2}},$$

and i is for the element under consideration, u for any other element, and u' for the mirroring element of u. The v is for the time retard of the current and charge on the core of the element u, and v' is for that of the mirroring element u'. The w is for the time retard of the charge diffused into the corona sheath of the

element u, and w' is for that of the mirroring element u'. The $\alpha_{u,v}$ is a coefficient for diffused charges in corona sheath of the element u at time v. Due to a uniform $dl_{i,j}/dz$ and $\lambda_{i,j}$ are assigned for each element, the contribution from these two terms to each element itself is zero. The $E_{i,j}$ represents the scatter field due to $dl_{i,j}/dt$ in equation (9). It takes a critical role to $I_{i,j}$ and needs to be treated carefully. By introducing a self-induction-like parameter $L_{i,j}$ instead of $E_{i,j}$, the $I_{i,j}$ can be solved based on equations (19) and (21) as

$$I_{i,j} = I_{i,j-1} e^{\frac{-\Delta t}{g_{i,j} L_{i,j}}} + g_{i,j}\left(E_i^A - E_{i,j}^C\right)\left(1 - e^{\frac{-\Delta t}{g_{i,j} L_{i,j}}}\right). \qquad (22)$$

where $g = 1/Z$ is the conductance. L is the self-induction-like parameter of the element under consideration, which is estimated as

$$L_{i,j} = \frac{\mu_0}{4\pi}\int_{-\frac{\Delta s}{2}}^{\frac{\Delta s}{2}} \frac{1}{\sqrt{r_{i,j}^2 + z^2}} dz = \frac{\mu_0}{4\pi}\ln\frac{\Delta s}{r_{i,j}}. \qquad (23)$$

where r is the channel core radius which evolves with time. The channel core heating (T—temperature) and expansion (V—volume and P—pressure) may follow a nonlinear relationship of $PV \sim nRT$, with the R might be a function of T at high temperature. The core conductivity (σ) depends the product of density (N_e) and mobility (v_e) of electrons. In general, a higher T causes a higher N_e but a lower v_e in ionized gas. There are many studies examining the electric conductivity as a function of the temperature, $\sigma(T)$, for various gases at high temperature. Based on computations [*Devoto*, 1967] and experiments [*Riaby et al.*, 2010], it is found that the σ increases linearly with T in the range of 6000–10,000°K in partially ionized argon. *Morris et al.* [1970] have measured the electric conductivities of hydrogen, nitrogen, and argon at temperatures up to 14,000°K. Their results also show that the σ is linear in T below 5000°K and has a change in slope at 8000°K above, for all these gases. Based on above research studies and for the first-order approximation, we take $PV \sim T$ and $\sigma \sim T$ and assume that V and P weight the same against the change of T, then we have $V^2 \sim \sigma$. For a unit length of channel, as $V = \pi r^2$ and $g = \pi r^2 \sigma$, $V^2 \sim \sigma$ means $r^6 \sim g$. As such, the core radius versus the core conductance can be approximated as

$$\frac{r_{i,j}}{r_0} = \left(\frac{g_{i,j}}{g_0}\right)^{\frac{1}{6}}. \qquad (24)$$

where g_0 is the initial channel conductance which is determined from the Z in equation (8). The r_0 is the initial channel core radius. In this study, $r_0 = 2.5$ mm corresponding to $g_0 = 2$ S/m is referred. Such an approximation may lead to a slower expansion of r versus g than the reality.

2.4.2. Evolution of the Channel Conductance
For the arcing process within the streamer gap, the evolution of conductance per unit length $g(t)$ and its numerical solution are based on the Toepler's spark law as [*Kumar et al.*, 2008]

$$g(t) = \frac{\int_0^t I \cdot dt}{C_t}, \quad g_{i,j} = \sum_{j'=1}^{j} I_{i,j'} \cdot \Delta t \, / \, C_t. \qquad (25)$$

where C_t is a constant of 0.02 Vs. Streamer gap channel will transfer into a leader channel when its conductance rises to that of the leader channel.

The variation of conductance per unit length of the leader channel (both DNL and UCL) is based on the first-order arc function as [*Rizk*, 1989]:

$$\frac{d}{dt}g(t) = \frac{g_\infty(I) - g(t)}{\theta}. \qquad (26)$$

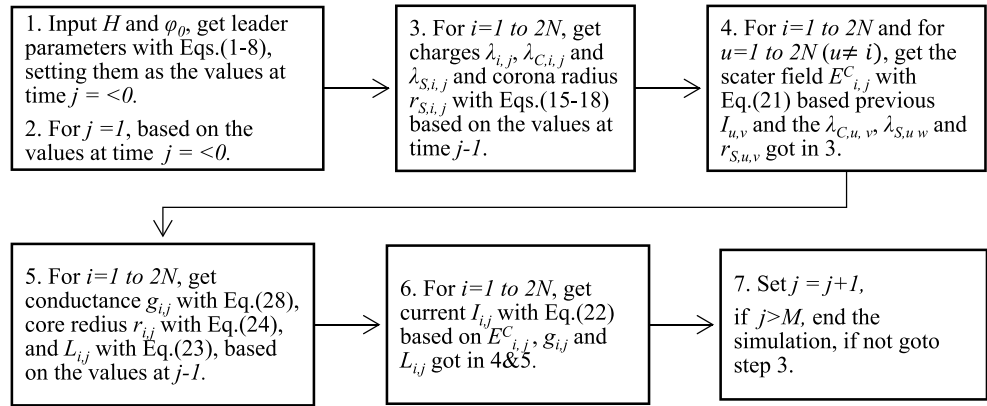| 1. Input H and φ_0, get leader parameters with Eqs.(1-8), setting them as the values at time $j = <0$. 2. For $j = 1$, based on the values at time $j = <0$.	3. For $i=1$ to $2N$, get charges $\lambda_{i,j}$, $\lambda_{C,i,j}$ and $\lambda_{S,i,j}$ and corona radius $r_{S,i,j}$ with Eqs.(15-18) based on the values at time j-1.	4. For $i=1$ to $2N$ and for $u=1$ to $2N$ $(u\neq i)$, get the scater field $E^C_{i,j}$ with Eq.(21) based previous $I_{u,v}$ and the $\lambda_{C,u,\,v}$, $\lambda_{S,u\,w}$ and $r_{S,u,v}$ got in 3.
5. For $i=1$ to $2N$, get conductance $g_{i,j}$ with Eq.(28), core redius $r_{i,j}$ with Eq.(24), and $L_{i,j}$ with Eq.(23), based on the values at j-1.	6. For $i=1$ to $2N$, get current $I_{i,j}$ with Eq.(22) based on $E^C_{i,j}$, $g_{i,j}$ and $L_{i,j}$ got in 4&5.	7. Set $j = j+1$, if $j>M$, end the simulation, if not goto step 3.

Figure 3. Flowchart of the algorithm for modeling of return stroke current.

where $g_\infty(I)$ is the maximum conductance that can be achieved at a steady current I and θ is a time constant for $g(t)$ to rise/fall to $g_\infty(I)$ at steady current condition. Based on model testing results, we propose

$$\theta = \begin{cases} \theta_r = 4 \sim 20\,\mu s & \text{for current rising stage} \\ \theta_f = 40 \sim 200\,\mu s & \text{for current falling stage} \end{cases}$$

We also propose

$$g_\infty(I) = I^{1+\alpha}/C_a. \tag{27}$$

where C_a is a constant of 50,000 W and α is a constant of 0.2–0.4 for cases of large impulsive current (like return stroke). For cases of small steady current (like leader), $C_a = C_b = 30,000$ W and $\alpha = 1$, as equation (6). For comparison, *Hutzler and Hutzler-Barre* [1978] in a leader propagation model proposed $\theta_r = 30$ μs, $\theta_f = 500$ μs, and the $\alpha = 0.4$. The numerical solution of equation (26) for the arc regime is then given by

$$g_{i,j} = g_{i,j-1}e^{\frac{-\Delta t}{\theta}} + g_\infty(I_{i,j-1})\left(1 - e^{\frac{-\Delta t}{\theta}}\right). \tag{28}$$
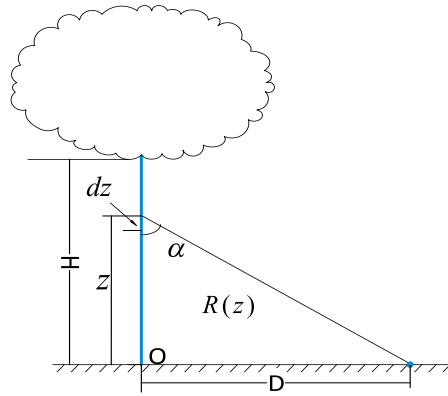
For easy understanding of the algorithm for modeling of the return stroke current, a flowchart is provided as in Figure 3.

3. Modeling of Light and Electromagnetic Emissions From Return Stroke

3.1. Electrical and Magnetic Fields From Return Stroke

As shown by Figure 4, with the simulated current, the vertical electric field produced by a return stroke on ground can be easily estimated as follows [*Cooray*, 2014]:

$$E_V(D,t) = \begin{bmatrix} \dfrac{1}{2\pi\epsilon_0}\displaystyle\int_0^H \dfrac{2 - 3\sin\alpha(z)^2}{R^3(z)}\int_0^t I\left(z,\tau - \dfrac{R(z)}{c}\right)d\tau\,dz \\[2ex] + \dfrac{1}{2\pi\epsilon_0}\displaystyle\int_0^H \dfrac{2 - 3\sin\alpha(z)^2}{cR^2(z)}\cdot I\left(z,t - \dfrac{R(z)}{c}\right)dz \\[2ex] - \dfrac{1}{2\pi\epsilon_0}\displaystyle\int_0^H \dfrac{\sin\alpha(z)^2}{c^2R(z)}\cdot \dfrac{\partial}{\partial t}I\left(z,t - \dfrac{R(z)}{c}\right)dz \end{bmatrix}. \tag{29}$$

$$\sin \alpha(z) = \frac{D}{\sqrt{D^2 + z^2}},$$

$$R(z) = \sqrt{D^2 + z^2}.$$

where $E_V(D, t)$ is the vertical electric field at point of P on ground. D is the distance from observation point P on ground to the lightning channel base.

The corresponding numerical solution is

Figure 4. Illustration of calculation of return stroke electromagnetic fields.

$$E_V(D,j) = \frac{\Delta s}{2\pi\epsilon_0} \sum_{i=1}^{N} \left[\begin{array}{c} \dfrac{2 - 3\sin\alpha_i^2}{R_i^3} \sum_{j'}^{j} I\left(i, j' - \dfrac{R_i}{c}\right) \\ + \dfrac{2 - 3\sin\alpha_i^2}{cR_i^2} I\left(i, j - \dfrac{R_i}{c}\right) \\ - \dfrac{\sin\alpha_i^2}{c^2 R_i \Delta t} \left(I\left(i, j - \dfrac{R_i}{c}\right) - I\left(i, j - \dfrac{R_i}{c} - 1\right) \right) \end{array} \right]. \tag{30}$$

Similarly, the horizontal magnetic field at point P on ground is given by [*Cooray*, 2014]

$$B_\phi(D,t) = \frac{1}{2\pi\epsilon_0 c^2} \int_0^H \left(\begin{array}{c} \dfrac{\sin\alpha(z)}{R^2(z)} I\left(z, t - \dfrac{R(z)}{c}\right) \\ + \dfrac{\sin\alpha(z)}{cR(z)} \dfrac{\partial}{\partial t} I\left(z, t - \dfrac{R(z)}{c}\right) \end{array} \right) dz. \tag{31}$$

The corresponding numerical solution is

$$B_\phi(D,j) = \frac{1}{2\pi\epsilon_0 c^2} \sum_{i=1}^{N} \left[\begin{array}{c} \dfrac{\sin\alpha_i}{R_i^2} I\left(i, j - \dfrac{R_i}{c}\right) + \\ \dfrac{\sin\alpha_i}{cR_i \Delta t} \left(I\left(i, j - \dfrac{R_i}{c}\right) - I\left(i, j - \dfrac{R_i}{c} - 1\right) \right) \end{array} \right]. \tag{32}$$

3.2. Light Emission From Return Stroke

According to energy conservation law, all energy that consumed by light, thunder, electromagnetic wave, and heating is from the input electric energy. The input electric power per unit length of channel segment is given by

$$P_e(z, t) = I(z, t)^2 / g(z, t). \tag{33}$$

Research studies show that about 10% of the electric power is released by light emission [*Guo and Krider*, 1983; *Quick and Krider*, 2013]. We assume that at any moment the power related to the channel heating and lighting is a fraction (C_l) of the total electric power as $C_l P_e$ and the lighting power is P_l. As such, the instant net power for channel heating is $C_l P_e - P_l$ and the channel accumulated heating energy will be $W_h = \int (C_l P_e - P_l) dt$. Physically, the light radiation power depends on the volume (or mass: Δm) fraction of air excited and the level of excitation (temperature: T) during the return stroke, i.e., $P_l \sim T \Delta m$
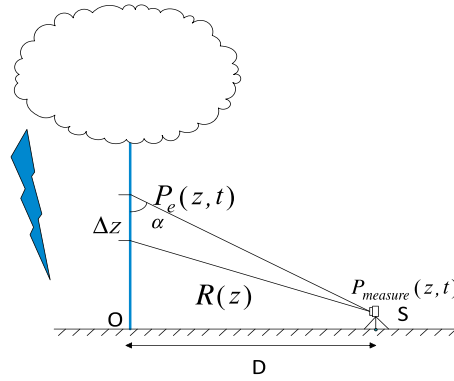
Figure 5. Illustration of calculation of return stroke light emissions.

[*Ma et al.*, 2011]. The channel rising temperature in turn depends on the accumulated heating energy and the heated mass, i.e., $W_h \sim (T - T_0) \Delta m$, where T_0 is the initial gas temperature. As such, the lighting power could be supposed to be proportional to the channel accumulated heating energy, i.e., P_l (z, t) $\sim W_h$ (z, t). Meanwhile, the light emission may make the channel cooling down after a certain time (θ_l) if the channel accumulated heating energy keeps no change. As such, the lighting power per unit length of channel can be related to the total input electric power as

$$P_l(z, t) = \frac{1}{\theta_l}\int_0^t (C_l P_e(z, \tau) - P_l(z, \tau)) d\tau. \tag{34}$$

where C_l is a numerical constant representing the percentage of the input electric power related to the channel heating and lighting and θ_l is a time constant reflecting the channel cooling down rate due to light emission, which is taken as the same as the θ_f in this study. The solution of equation (25) is

$$P_l(z, t) = \frac{C_l}{\theta_l} e^{-\frac{t}{\theta_l}}\int_0^t P_e(z, \tau) e^{\frac{\tau}{\theta_l}} d\tau. \tag{35}$$

Assuming that the light source is isotropic (Figure 5), for a light sensor at point S with an exposure time ΔT and a channel section view of $z \sim z + \Delta z$, the light power at the sensor per unit area is

$$P_m(D, z, t) = \frac{1}{\Delta T \Delta z}\int_z^{z+\Delta z}\int_{t-\Delta T}^t \frac{\sin \alpha(z')}{4\pi R(z')^2} P_l\left(z', \tau - \frac{R(z')}{c}\right) d\tau dz'. \tag{36}$$

Table 1. Initial Parameters for Leader-Return Stroke Modeling

Symbol	Quantity	Value
E_{C0}	Critical negative electric field at ground (equation (4))	−750 kV/m
E_{C0+}	Critical positive electric field at ground (equation (4))	+500 kV/m
C_b	Leader power constant (equation (6))	30,000 W/m
C_t	Streamer heating up constant (equation (25))	0.02 Vs
θ_r	Time constant for rising conductance (equation (26))	5 μs
θ_f	Time constant for falling conductance (equation (26))	50 μs
C_a	Return stroke power constant (equation (27))	50,000 W/m
α	Power index for large current for equation (27)	0.2
C_l	Coefficient of energy for lighting (equation (34))	0.1
θ_l	Time constant for lighting (equation (34))	50 μs
r_0	Initial reference channel radius (equation (24))	2.5 mm
g_0	Initial reference channel conductance (equation (24))	2 S/m
Δs	Channel segment length for computing	2.4 m
Δt	Time step interval for computing	4 ns
ϵ_0	Free space permittivity ($C^2/m^2/N$)	8.86×10^{-12}
μ_0	Free space permeability (H/m)	$4\pi \times 10^{-7}$
σ_S	Line conductivity of corona sheath (equation (13))	10 μS/m

Table 2. The Modeled Later Stage Leader Parameters With Different Cloud Initiation Potentials

Cloud Potential φ_0 (MV)	Channel Height H (m)	Streamer gap Ds (m)	UCL Length D_{UL} (m)	DNL E-Field E_{DL} (V/m)	UCL E-Field E_{UL} (V/m)	DNL Resistance Z_{DL} (Ω/m)	UCL Resistance Z_{UL} (Ω/m)	Streamer Resistance Z_{ST} (Ω/m)	DNL Current I_{DL} (A)	DNL Core Radius r_0 (mm)
−10	300	9.6	2.4	7,816	23,955	1,721	19,129	179,665	4.17	0.64
−20	1,200	21.6	4.8	2,537	8,458	214	2,385	63,433	11.8	0.91
−30	2,400	36	7.2	1,380	4,600	63.5	705	34,500	21.7	1.12
−40	3,600	48	12	895	2,986	26.7	294	22,396	33.5	1.28
−50	4,800	62.4	14.4	640	2,136	13.6	152	16,018	46.8	1.44
−60	6,000	76.8	16.8	487	1,624	7.9	88	12,180	61.6	1.58
−70	7,200	88.8	21.6	386	1,288	5	55.3	9,663	77.6	1.70
−80	9,000	103.2	24	316	1,054	3.3	37.5	7,907	94.8	1.83
−90	9,600	115.2	28.8	265	883	2.3	26	6,625	113	1.94
−100	12,600	129.6	31.2	226	754	1.7	19	5,655	132.6	2.04
−110	14,400	144	33.6	196	653	1.3	14.2	4,901	153	2.13
−120	16,200	156	38.4	172	573	1	11	4,300	174.4	2.22
−130	18,000	170.4	40.8	152	508	0.78	8.6	3,813	196.7	2.32
−140	19,600	182.4	45.6	137	455	0.62	6.9	3,412	219.8	2.42

4. Modeling Results

With the present model and the initial values in Table 1, we have studied the evolution of the current and the light and electromagnetic emissions of a leader-return stroke with different initiation potentials (φ_0). There are totally 14 cases studied, with φ_0 ranges from −10 to −140 MV in an interval of −10 MV.

Table 2 shows the leader parameters (initial values of return stroke channels) corresponding to the 14 cases, which are calculated with the leader model in section 2.2 and the initial values in Table 1.

The channel height ($H + H'$) is determined in a way that the return stroke current decays to about zero when it arrives at the upper end of the channel. The current of UCL is set to $0.3I_{DL}$ and that of the streamer gap is set to vary from I_{DL} when at DNL tip down to $0.3I_{DL}$ when at UCL tip. The streamer resistance shown in the table is for that when the streamer current equals I_{DL} for reference purpose. As can be seen from the table, the higher of the initiation potential, the longer of the lightning channel and the streamer gap as well as the UCL, and the larger of the leader current. With the return stroke model in section 2.3 and the leader parameters in Table 2, simulations of the return stroke parameters for the 14 cases have been done. Since the property of return stroke parameters for all the 14 cases are similar to each other, in following, we take the case $\varphi_0 = -50$ MV as an example to illustrate details of the property of return stroke parameters.

4.1. Return Stroke Current and Conductance

Shown in Figure 6 are the variations of current, channel conductance, channel core radius, and the charge accumulation with time and height for the return stroke of case $\varphi_0 = -50$ MV. The initial channel condition is the channel length $H = 4800$ m, UCL length $D_{UL} = 14.4$ m, streamer gap $D_{ST} = 62.4$ m, DNL current $I_{DL} = 46.8$ A, and DNL core radius $r_0 = 1.44$ mm.

As shown in the figure, the initial negative charge (λ_L in equation (1)) in the leader corona sheath shows first an increase from the zero when at the ground level to its maximum of about −0.65 mC/m when near the connecting point (about 77 m high), and then a decrease to about −0.18 mC/m when at 4.8 km high. Similarly, the positive charge (λ in equation (12)) accumulated along the channel by the return stroke shows first an increase from the zero when at the ground level to its maximum of about +0.35 mC/m when near the connecting point, and then a decrease to about +0.18 mC/m when at 4.8 km high. The diffusing current peak also shows first an increase from the zero when at ground level to its maximum of about 235 A/m when near the connecting point, and then a decrease to about 17 A/m when at 4.8 km high.

Table 3 is a statistics of the current waveform, return stroke speed, and channel conductance along the channel for this case. Both the current amplitude and its propagation speed decrease exponentially while the current waveform becomes flatter and wider, with the increase of the height. The current peak (I_p) is 60 kA when near ground and decreases to 9 kA when at 4.8 km high. The return stroke speed (v_r), which is measured using
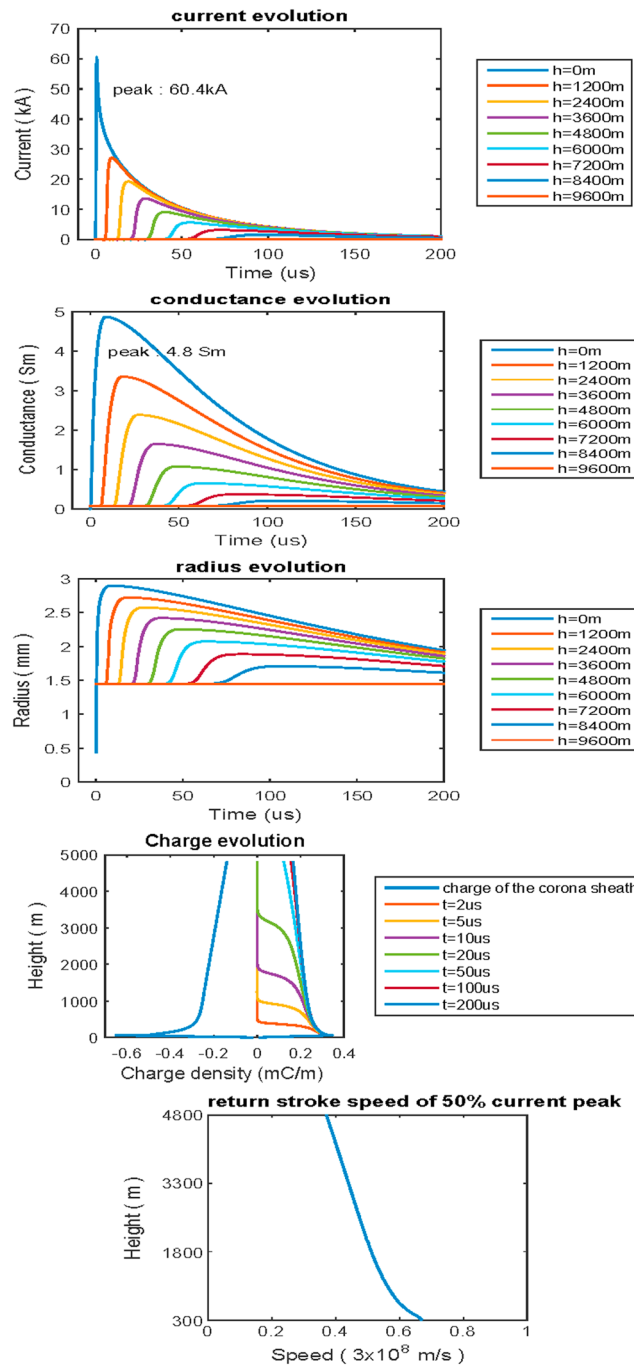
Figure 6. The spatial and temporal evolution of the return stroke current, channel conductance, core radius, the charge deposit, and the return stroke speed for the return stroke for case $\varphi_0 = -50$ MV.

the 50% peak of the current wave, is 2.0×10^8 m/s when near ground and decreases to 1.1×10^8 m/s when at 4.8 km high, which is within the range of observed return stroke speed in the literature. The current waveform has a 10% to 90% rising time (T_r) of 0.3 μs when near ground and 4.9 μs when at 4.8 km high. The full width at half maximum (FWHM) is 8.5 μs when near ground and 53.7 μs when at 4.8 km high. The channel core expands from the initial 1.4 mm to 2.9 mm in radius. The amplitude of both the channel conductance and core radius decreases exponentially while their waveform becomes flatter and wider, with the increase of the height. Especially, *Shao et al.* [2012] studied the behavior of return stroke current based on the remotely detected electric field change waveform. Their results showed that the return stroke current traveled in a dispersive and lossy manner, which are well consistent with the present results.

Figure 7 is an expansion of the current in Figure 6 but focuses on the rising front of the current along the channel below 150 m, where the attachment process occurs. As shown in the figure, the current front first appears at $h = 45.6$ m which is the middle of the streamer gap and then moves in two directions. One wave moves upward from $h = 45.6$ m (middle of streamer gap) to $h = 60$ m, then $h = 76.8$ m (tip of DNL) and then $h = 91.2$ m, with an average speed of 0.5 speed of light. One wave moves downward from $h = 45.6$ m to 31.2 m, then $h = 14.4$ m (tip of UCL) and then $h = 0$ m, with an aver-

age speed of 0.4 speed of light. As the downward wave reaches the ground, it is reflected to move upward with a speed of 0.68 speed of light and its amplitude is doubled. Such a two-current wave attachment process is well consistent with the observations by *Wang et al.* [2014].

4.2. Electrical and Magnetic Fields From Return Stroke

Figure 8 shows the calculated electrical and magnetic fields at different distances on ground, for the return stroke of case $\varphi_0 = -50$ MV. The calculation is based on the current shown in Figure 6 with the model in

Table 3. Statistics of Modeled Current and Speed and Channel Conductance for the Return Stroke for Case $\varphi_0 = -50$ MV

Channel Altitude z (m)	Rising Front T_r (μs)	Full Wave Width FWHM (μs)	Current Peak I_p (kA)	Return Speed v_r/c	Conduct. Peak g_p (Sm)	Core Peak Radius r_p (mm)
0	0.31	8.49	60.42	-	4.83	2.90
60	0.46	10.91	55.26	0.68	4.78	2.87
600	0.79	25.70	33.90	0.61	3.98	2.80
1200	1.49	31.40	27.09	0.55	3.34	2.72
1800	2.09	34.93	22.74	0.51	2.83	2.65
2400	2.61	37.95	19.25	0.48	2.38	2.57
3000	3.09	41.01	16.25	0.45	1.99	2.50
3600	3.60	44.44	13.59	0.43	1.64	2.42
4200	4.18	48.54	11.21	0.40	1.34	2.34
4800	4.88	53.72	9.08	0.37	1.07	2.25

section 3.1. It should be pointed out that there is a little difference in the electromagnetic field calculated when only the lower half channel H is considered with that when the whole channel $H + H'$ is considered. It is noted that at a distance less than 1000 m the waveform of the magnetic field is quite similar to that of the channel base current. This implies that we may sense the return stroke current with magnetic field measurements at a close distance. The properties of waveform of modeled electrical and magnetic fields versus distance are well consistent with those in the literature.

4.3. Light Emissions From Return Stroke

Figure 9 shows the modeled light power per unit channel length (Figure 9, left) and the return stroke speed based on light power (Figure 9, right) versus the height respectively, for the return stroke of case $\varphi_0 = -50$ MV. The calculation is based on the current and conductance shown in Figure 6 with equation (35) in section 3.2. The light power peak is 99.1 MW/m when at the channel base and decays sharply to 9.6 MW/m when at 4.8 km high, which are comparable to the estimates of *Guo and Krider* [1983] and *Quick and Krider* [2013]. The return stroke speed here is determined based on the median of the rising front of the light power waveform, which is very like that determined based on the current waveform as shown in Figure 6. The return stroke speed has a trend of decreasing as it propagates upward, which is consistent with the observation results of triggered lightning by *Wang et al.* [1999].

Figure 10 is an expansion of the rising front of the calculated light power in Figure 9 but focuses on the height below 150 m, where the attachment process is supposed to occur. Similar to the current rising front shown in Figure 7, the rising front of the light power also starts with 2 light waves. One light wave moves upward from $h = 45.6$ m (middle of the streamer gap) to $h = 76.8$ (tip of DNL) and then $h = 91.2$ m, at about 0.5 speed of light. One light wave moves downward from $h = 45.6$ m to $h = 14.4$ m (tip of UCL) and then $h = 0$ m (the ground), at about 0.4 speed of light. The downward wave reflects at ground and goes upward at 0.65 speed of light. These results are well consistent with the observed attachment processes in triggered lightning discharge by *Wang et al.* [2014].

Figure 11 shows the modeled light power detected by a sensor with unit area at 5 km to the channel base on ground with different time and space revolutions, for the return stroke of case $\varphi_0 = -50$ MV. The calculation is based on the light power in Figure 9 with equation (36) in section 3.2. It is obvious that the light waveform
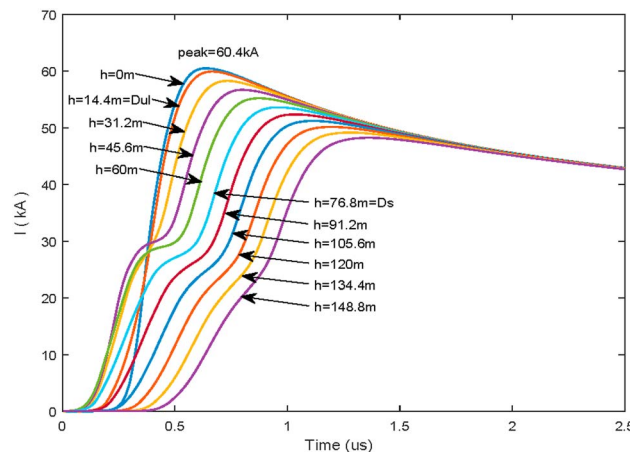

Figure 7. The rising front of the current along the channel below 150 m where the attachment occurs, expanded from Figure 6, for case $\varphi_0 = -50$ MV.
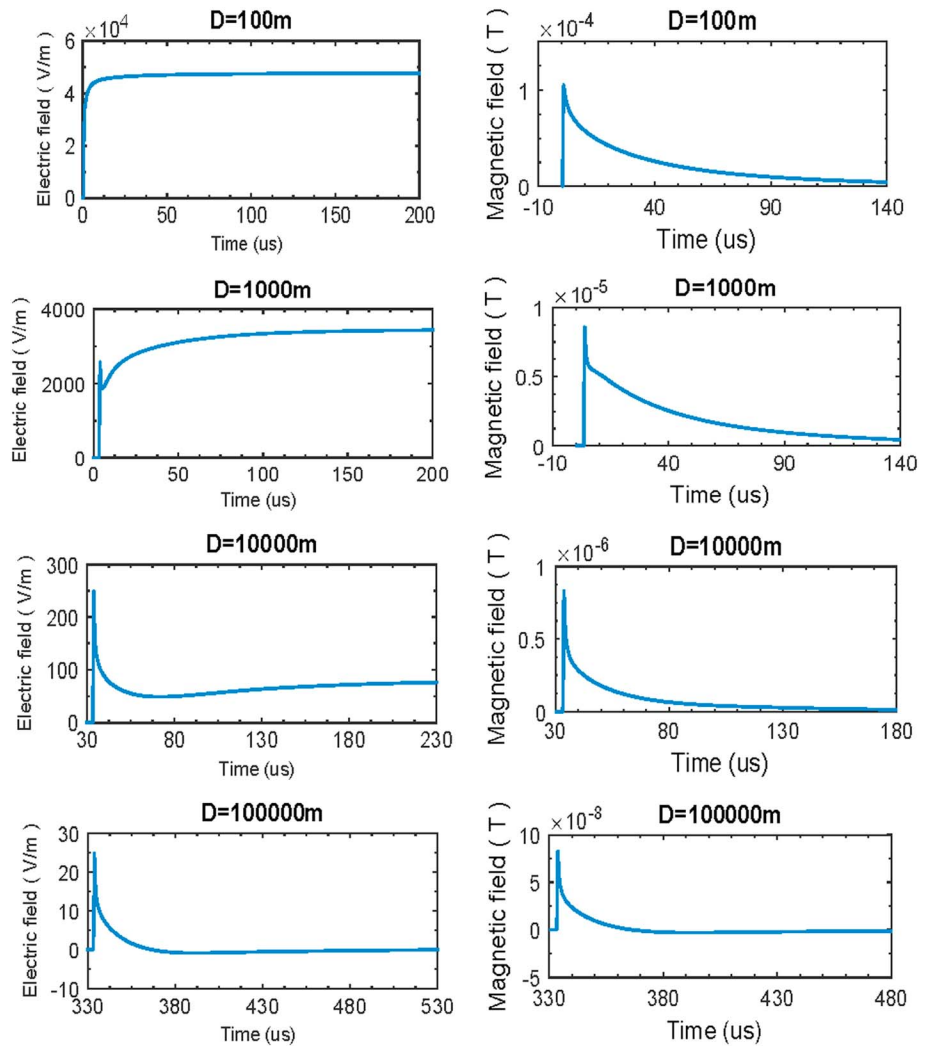
Figure 8. The calculated (left) electrical and (right) magnetic fields at different distance on ground, for the return stroke for case $\varphi_0 = -50$ MV.
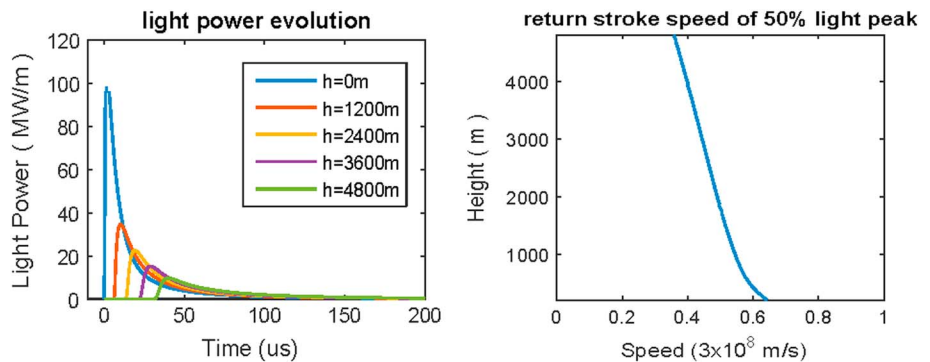

Figure 9. Calculated (left) light power per unit channel length versus time and height, and the (right) return speed based on the light waveform for the return stroke for case $\varphi0 = -50$ MV.
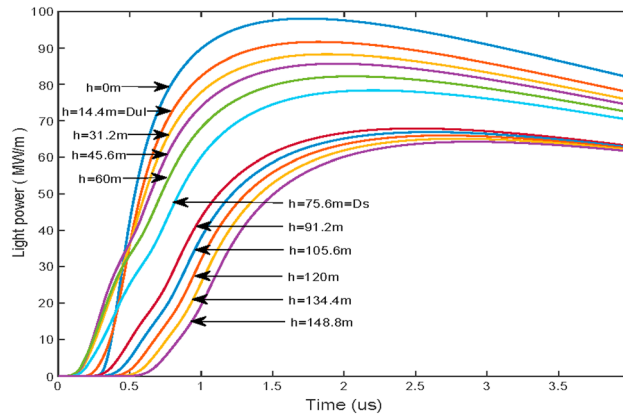
Figure 10. Expansion of the rising front of light power in Figure 9 for the channel below 150 m where the attachment process occurs, for case $\varphi_0 = -50$ MV.

detected by a sensor varies with the sensor time and space resolutions. The longer the exposure time of the sensor, the wider the light waveform it detected. And also the longer the channel segment viewed by the sensor, the wider the light waveform it detected. These results can well explain those observed light waveforms of return strokes in literature [*Wang et al.*, 2005; *Zhou et al.*, 2014].

Shown in Figure 12 is a comparison of the light waveform at a sensor with an exposure time $\Delta T = 8$ ns and a channel view $\Delta z = 10$ m and 200 m, respectively, with the current
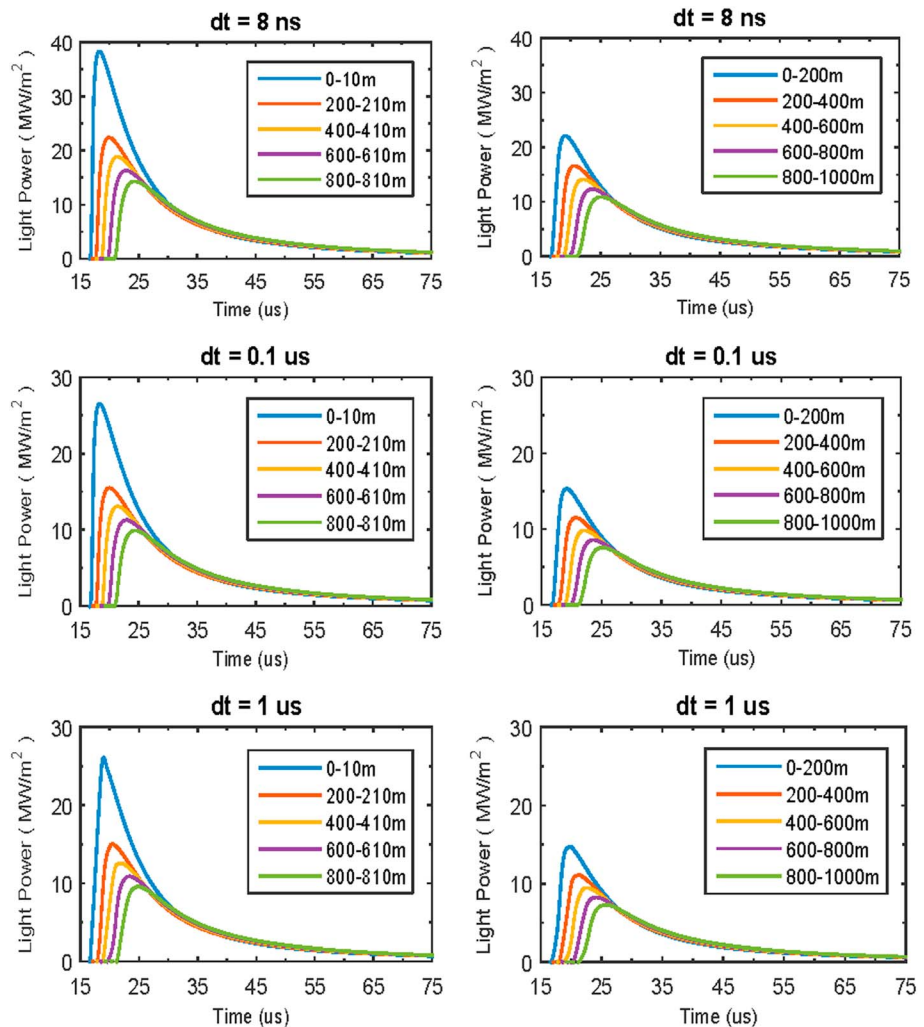

Figure 11. Calculated light power per unit area at a sensor with different exposure times (ΔT) and space views (Δz) at a distance of $D = 5$ km on ground, for the return.
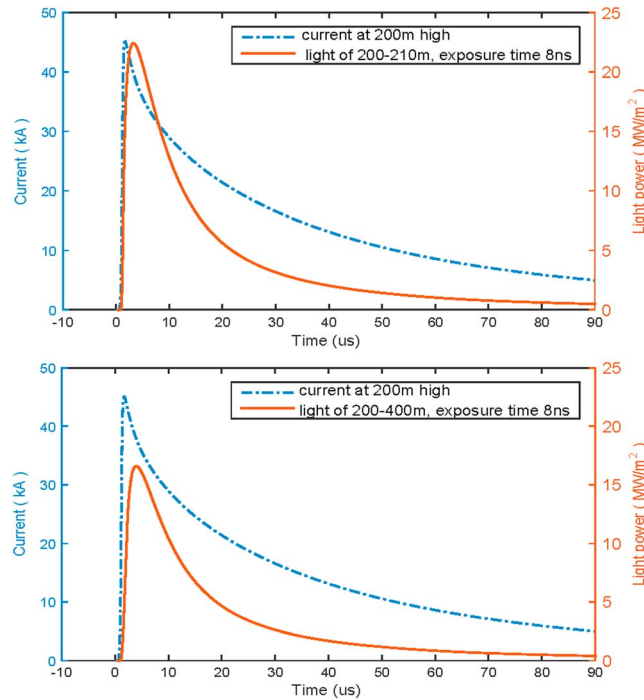
Figure 12. Comparisons of the light waveform of a sensor at exposure time $\Delta T = 8$ ns and channel view (top) $\Delta z = 200$–210 m and (bottom) 200–400 m respectively, with the current waveform at the channel height $z = 200$ m, for the return stroke for case $\varphi_0 = -50$ MV.

waveform, for the height of $z = 200$ m, for case $\varphi_0 = -50$ MV. It shows that the rising front of light waveform is slower than that of the current, even the exposure time and the space view of the sensor are very small. The larger the space view and exposure time, the slower the rising front of the light waveform than that of the current.

Wang et al. [2005] and *Zhou et al.* [2014] compared the current and optical signal with a high speed detection system for triggered lightning discharges. They found that the rising front of the current is always faster than that of the optical signal, which are well consistent with our simulation results.

Table 4 is a summary of the current peak (I_p), return stroke speed (v_r), conductance peak (g_p), core radius peak (r_p), and light power density peak (P_{lp}) along the channel up (z), and the electrical (E_{p100}) and magnetic (B_{p100}) field peaks at 100 km, for all the 14 cases. The first figure in columns 2–5 and 8 is the value at ground level, and the second one is that at the upper end of channel H. In overall, the larger the initiation potential φ_0 is, the larger the H, I_p, and v_r. For example, $\varphi_0 = -10$ MV corresponds to $H = 300$ m, $I_p = 2.6$ kA, and $v_r = 0.21c$ (at channel base), while $\varphi_0 = -140$ MV corresponds to $H = 19.8$ km, $I_p = 209$ kA, and $v_r = 0.86c$. The case 2.6 kA might be about the smallest return stroke available in a thunderstorm on Earth, while the case 209 kA might be about the strongest one. For each case, all the I_p, v_r, g_p, and P_{lp} show an exponentially deceasing trend with the increase of the height.

Table 4. Summary of Modeled Return Stroke Parameters Corresponding to Different Cloud Initiation Potentials

φ_0 (MV)	I_p (kA)	v_r (3×10^8 m/s)	g_p (Sm)	r_p (mm)	E_{p100} (V/m)	B_{p100} (10^{-9} T)	P_{lp} (MW/m)
−10	2.6–0.3	0.21–0.00	0.05–0.017	1.35–1.13	0.56	1.9	4.76–0.58
−20	10.2–0.8	0.31–0.04	0.35–0.057	1.87–1.38	2.61	8.7	22.4–1.24
−30	23.8–1.7	0.50–0.15	1.15–0.16	2.28–1.64	7.13	23.8	48.7–2.23
−40	41.8–4.5	0.63–0.26	2.70–0.47	2.63–1.96	15.4	51.3	79.3–5.28
−50	60.4–9.1	0.68–0.37	4.86–1.07	2.90–2.25	24.8	82.7	99.1–9.62
−60	76.1–13.4	0.74–0.44	7.00–1.73	3.08–2.44	33.3	111	128–12.9
−70	94.4–20.2	0.77–0.53	9.70–2.85	3.25–2.65	43.3	144	150–17.9
−80	109.5–23.5	0.80−−0.58	12.2–3.52	3.38–2.75	51.8	173	167–19.0
−90	127.3–28.9	0.81–0.60	15.3–4.60	3.51–2.87	61.7	206	185–21.7
−100	142.1–32.7	0.82–0.64	18.1–5.47	3.61–2.96	70.7	234	199–22.8
−110	159.6–38.5	0.84–0.69	21.5–6.78	3.71–3.06	79.8	266	213–25.3
−120	177.0–44.5	0.85–0.71	25.0–8.20	3.81–3.16	88.3	298	227–27.7
−130	191.5–48.9	0.85–0.74	28.0–9.37	3.88–3.23	97.4	324	237–28.7
−140	209.0–55.1	0.86–0.76	31.7–11.0	3.96–3.32	106.7	356	248–30.9

5. Conclusion and Discussion

Based on the macroscopic model concept of *Kumar et al.* [2008], a modified electromagnetic-physical model for first lightning return stroke is proposed. The model is modified in following four aspects.

1. The bidirectional leader concept [*Chen et al.*, 2013] and the attachment process [*Tran and Rakov*, 2015] are introduced into the model. The results of a self-organized downward negative leader (DNL) model [*Xu and Chen*, 2013] are applied as the initial state of the return stroke channel. For a given channel root potential in the cloud, the leader model provides parameters such as the striking distance and the current, longitudual electric field, conductance, charge quantity, and radius of the leader channel just before the return stroke, which are taken as the initial state of the return stroke channel. Besides, based on the difference of critical electric field between negative and positive polarities, an upward connecting leader (UCL) corresponding to a DNL is defined, and the two-current-wave phenomena (during the attachment process) at the return stroke starting stage is successfully simulated. It should be mentioned that the two-wave propagation phenomenon was well analyzed in works of *Raysaha et al.* [2012], but for cases of lightning strokes to tall grounded objects. Our works here aims to make the modeling of leader, attachment, and return stroke process be self-consistent.

2. The evolution mode of channel conductance, which is the most important parameter in the model, is further modified. *Kumar et al.* [2008] used the Toepler's spark law and the first-order arc function for the channel conductance for the streamer and arcing regimes, respectively. For rising current, they used equation $dg/dt = (g_\infty - g)/\theta_r$, but for falling current they used equation $dg/dt = -g/\theta_f$. This means that (i) the channel conductance increases as the current increases and decreases as the current decreases and (ii) the conductance is independent of the channel current at its falling stage, no matter it is below or above the g_∞ at the moment. Since both are empirical laws based on spark discharges in laboratory, modifications of them against lightning are necessary. Based on comparisons of simulated return stroke currents and those reported in the literature, we propose to use the same equation (26), $dg/dt = (g_\infty - g)/\theta$, for both the rising and falling stages of the channel conductance. This means that the conductance will keep to increase unless it becomes equal or larger than the g_∞ at the moment. Besides, we propose to take the factor α in equation (27) as 1.0 and 0.2 for leader and return stroke channels, respectively. Ranges of the simulated channel conductance with these modifications are qualitatively reasonable when compared with those in the literature.

3. The evolution of channel core radius versus the channel core conductance is introduced. The lightning channel core is consisted of high-temperature air plasma. The radius of the channel core depends on the plasma pressure, temperature, and mass density of the core. In general, the return stroke channel core may have a nonlinear relationship that $PV \sim nRT$ (where P is pressure, V is volume, T is temperature, and R is a constant related to specific gases, which might be a function of T when the temperature is very high) and P may tend to keep balance with the surrounding air. As the first-order approximation, we assume that the R keeps constant and P and V are equally weighted versus T. The temperature links to the channel ionization degree and hence the conductivity, while the volume links to the channel core radius. As such, the channel core radius is related to the channel conductance as shown by equation (24). Such a linear gas approximation may lead to a slower expansion of the core radius than the reality. Further modification and testing of the equation (24) are needed.

4. An alternative digitizing and solving approach for the time domain electric field integral equation (TD-EFIE) is proposed. Since TD-EFIE includes both differential and integral terms and varies with both space and time, digitizing process of the equation has significant impact on the solution accuracy. A popular digitizing solution for TD-EFIE is the quadratic space and time interpolation function by *Miller et al.* [1973], which can accurately evaluate the dependent variables in TD-EFIE at any point in the spacetime cone with a mild restriction on the space and time sample density. In the Miller's function, a singly connected wire structure is divided into a number of segments ($i = 1,\ldots,N$), each with a space length of Δs and centered at s_i. The time domain is also divided into a number of elements ($j = 1,\ldots,M$), each with a time interval of Δt and centered at t_j. A current I_{ij} is defined for the spacetime point centered at s_i and t_j. The current distribution within the segment i around time j, $I_{ij}(s', t')$ is then determined with the nine-point quadratic interpolation method in space and time dimensions. To avoid interpolation into the future, the current at time step j is interpolated backward to time steps $j - 1$ and $j - 2$ when $(s' - s_i)/c\Delta t < 0.5$. Otherwise, the interpolation in time is from time step j to $j + 1$ and $j - 1$. The space interpolation is from

segment i to $i + 1$ and $i - 1$ (see page 31 of *Miller et al*. [1973]). As such, the self-term of current-time-derivative $(dI/dt)_{ij}$ for a segment at time j is actually expressed as a complicated function of the current in the concerned segment at times j, $j - 1$ and $j - 2$ as well as that in its neighbor segments. In contrast, in the present method, we use the conventional digitizing approach that the channel is directly divided into many small elements, each is assigned with a uniform current along the element. The time step Δt is strictly related to the space element Δs by $\Delta s = 2c\Delta t$ for better accuracy. In particular, both $(dI/dt)_{ij}$ and I_{ij} terms in the equation are kept as what they are to form a matrix differential equation like: $L_{ij}(dI/dt)_{ij} + Z_{ij}I_{ij} = E^A_i - E^C_{ij}$, as shown by equations (19)–(21). The I_{ij} can then be analytically solved out as a function of (L_{ij}, Z_{ij}, E^A_i, and E^C_{ij}), as shown by equations (22) and (23). With such special treatments, the computing efficiency is significantly enhanced without losing the accuracy.

Besides, based on the current and conductance outputs of TD-EFIE model, an approach for simulating the electromagnetic field and optical signal of a return stroke is proposed and tested, as shown by equations (30)–(32) and equations (33)–(36), respectively. The simulated light waveform versus the current waveform can well explain the observation results of *Wang et al*. [1999, 2005, 2014].

Moreover, with above models, simulations of the current and electromagnetic and optical signals of a return stroke are performed for different initiation potentials in the range of −10 MV to −140 MV, resulting in different channel heights (ranging from 300 m to 20 km), current peaks (ranging from 2.6 to 209 kA), return stroke speed peaks (ranging from 0.2c to 0.8c), and light power peaks (ranging from 4.76 to 248 MW/m). The larger of the initiation potential, the larger of the channel height, current, return stroke speed, and light power. Both the current peak and its propagation speed attenuate exponentially as it propagates upward. All these results are qualitatively and quantitatively consistent with those reported in literature [*Guo and Krider*, 1983; *Quick and Krider*, 2013; *Shao et al*., 2012; *Wang et al*., 1999, 2014].

References

Baum, C. E., and L. Baker (1990), Analytic return-stroke transmission-line model, in *Lightning Electromagnetics*, edited by R. L. Gardner, pp. 17–40, Hemisphere, New York.

Berger, K. (1975), Parameters of lightning flashes, *Electra*, *41*, 23–37.

Chen, M., and Y. Du (2009), Possible impacts of earthing path impedance on lightning return stroke currents, *HKIE Trans*., *16*(1), 7–13, doi:10.1080/1023697X.2009.10668145.

Chen, M., X. Gou, and Y. Du (2013), The effect of ground altitude on lightning striking distance based on a bi-directional leader model, *Atmos. Res*., *125–126*, 76–83.

Cooray, V. (2014), *The Lightning Flash*, The Institution of Engineering and *Technology*, London.

Devoto, R. S. (1967), Transport coefficients of partially ionized argon, *Phys. Fluids*, *10*, 354–364, doi:10.1063/1.1762115.

Du, Y., and M. Chen (2010), Influence of building structures on the lightning return stroke current, *IEEE Trans. Power Del*., *25*(1), 307–315, doi:10.1109/TPWRD.2009.2035420.

Du, Y., X. H. Wang, and M. Chen (2012), Circuit parameter of vertical wires above a lossy ground in PEEC models, *IEEE Trans. EMC*, *54*(4), 871–879, doi:10.1109/TEMC.2011.2174240.

Fuchs, F., E. U. Landers, R. Schmid, and J. Wiesinger (1998), Lightning current and magnetic field parameters caused by lightning strikes to tall structures relating to interference of electronic systems, *IEEE Trans. EMC*, *40*, 444–451.

Gorin, B. N., and V. I. Markin (1975), Lightning return stroke as a transient process in a distributed system, *Trudy ENIN*, *43*, 114–130.

Guo, C., and E. P. Krider (1982), The optical and radiation field signatures produced by lightning return strokes, *J. Geophys. Res*., *87*, 8913–8922, doi:10.1029/JC087iC11p08913.

Guo, C., and E. P. Krider (1983), The optical power radiated by lightning return strokes, *J. Geophys. Res*., *88*, 8621–8622, doi:10.1029/JC088iC13p08621.

Hutzler, B., and D. Hutzler-Barre (1978), Leader propagation model for predetermination of switching surge flashover voltage of large air gaps, *IEEE Trans. Power Apparatus Syst*., 1087–1096.

Idone, V. P., and R. E. Orville (1982), Lightning return stroke velocities in the Thunderstorm Research International Program (TRIP), *J. Geophys. Res*., *87*, 4903–4916, doi:10.1029/JC087iC07p04903.

Kumar, U., and R. B. Raysaha (2013), Genesis of return stroke current evolution at the wavefront, *Atmos. Res*., *29*, 42–48.

Kumar, U., R. B. Raysaha, and K. Kumar (2008), Time domain modelling of first return stroke of lightning, *Open Atmos. Sci. J*., *2*, 261–270.

Lin, Y., M. Uman, and R. Standler (1980), Lightning return stroke models, *J. Geophys. Res*., *85*, 1571–1583, doi:10.1029/JC085iC03p01571.

Ma, S., J. Howard, and N. Thapar (2011), Relations between light emission and electron density and temperature fluctuations in a helium plasma, *Phys. Plasmas*, *18*, 083301, doi:10.1063/1.3620403.

Maslowski, G., and V. A. Rakov (2006), A study of the lightning channel corona sheath, *J. Geophys. Res*., *111*, D14110, doi:10.1029/2005JD006858.

Mazur, V., and L. H. Ruhnke (1998), Model of electric charges in thunderstorms and associated lightning, *J. Geophys. Res*., *103*, 23,299–23,308, doi:10.1029/98JD02120.

McCann, G. (1944), The measurement of lightning currents in direct strokes, *Electr. Eng*., *63*, 1157–1164.

Miller, E. K., A. J. Poggio, and G. J. Burke (1973), An integral equation technique for the time-domain analysis of thin wire structure. Part I: The numerical method, *J. Comput. Phys*., *12*, 24–48.

Moini, R., V. A. Rakov, M. A. Uman, and B. Kordi (1997), An antenna theory model for the lightning return stroke, *Proc. 12th Int. Symp. On Electromagnetic Compatibility*, Zurich, Switzerland.

Morris, J. C., R. P. Rudis, and J. M. Yos (1970), Measurements of electrical and thermal conductivity of hydrogen, nitrogen, and argon at high temperatures, *Phys. Fluids*, *13*, 608–617, doi:10.1063/1.1692966.

Pinto, O., I. Pinto, M. Saba, N. Solorzano, and D. Guedes (2005), Return stroke peak current observations of negative natural and triggered lightning in Brazil, *Atmos. Res.*, *76*, 493–502.

Plooster, M. N. (1970), Shock waves from line sources. Numerical solutions and experimental measurements, *Phys. Fluids*, *13*, 2665–2675.

Plooster, M. N. (1971), Numerical simulation of spark discharges in air, *Phys. Fluids*, *14*, 2111–2123.

Podgorski, A. S., and J. A. Landt (1987), Three-dimensional time domain modeling of lightning, *Power Eng. Rev. IEEE*, 72–73.

Popov, N. A. (2003), Formation and development of a leader channel in air, *Plasma Phys. Rep.*, *29*, 695–708.

Quick, M. G., and E. P. Krider (2013), Optical power and energy radiated by natural lightning, *J. Geophys. Res. Atmos.*, *118*, 1868–1879, doi:10.1002/jgrd.50182.

Raizer, Y. P. (1991), *Gas Discharge Physics*, Springer, Berlin.

Rakov, V. A. (1997), Lightning electromagnetic fields: Modeling and measurements, *Proc. 12th Int. Symp. On Electromagnetic Compatibility*, pp. 59–64, Zurich, Switzerland.

Rakov, V. A. (1998), Some inferences on the propagation mechanisms of dart leaders and return strokes, *J. Geophys. Res.*, *103*(D2), 1879–1887, doi:10.1029/97JD03116.

Rakov, V. A., and M. A. Uman (1998), Review and evaluation of lightning return stroke models including some aspects of their application, *IEEE Trans. EMC*, *40*, 403–426.

Rakov, V. A., and M. A. Uman (2003), *Lightning: Physics and Effects*, pp. 143–163, Cambridge Univ. Press, New York.

Raysaha, R. B., U. Kumar, and R. Thottappillil (2011), A macroscopic model for first return stroke of lightning, *IEEE Trans. EMC*, *53*, 782–791, doi:10.1109/Temc.2010.2090663.

Raysaha, R. B., U. Kumar, and V. Cooray (2012), Analysis for the reflected waves transmitted on to the channel by tall grounded objects using a special case, *IEEE Trans. EMC*, *54*(2), 262–271.

Riaby, V. A., V. P. Savinov, A. V. Patzioral, and D. P. Tkachenko (2010), Evaluation of the mean argon plasma conductivity and temperature at the exit of an atmospheric DC arc plasma torch, *J. Phys. Conf. Ser.*, *223*, 012007, doi:10.1088/1742-6596/223/1/012007.

Riousset, J. A., V. P. Pasko, P. R. Krehbiel, R. J. Thomas, and W. Rison (2007), Three dimensional fractal modeling of intracloud lightning discharge in a New Mexico thunderstorm and comparison with lightningmapping observations, *J. Geophys. Res.*, *112*, D15203, doi:10.1029/2006JD007621.

Rizk, F. A. M. (1989), A model for switching impulse leader inception and breakdown of long air-gaps, *IEEE Trans. Power Del.*, *4*, 596–606.

Shao, X.-M., E. Lay, and A. R. Jacobson (2012), On the behavior of return stroke current and the remotely detected electric field change waveform, *J. Geophys. Res.*, *117*, D07105, doi:10.1029/2011JD017210.

Tran, M. D., and V. A. Rakov (2015), When does the lightning attachment process actually begin ?, *J. Geophys. Res. Atmos.*, *120*, 6922–6936, doi:10.1002/2015JD023155.

Wang, D., N. Takagi, T. Watanabe, V. Rakov, and M. Uman (1999), Observed leader and return-stroke propagation characteristics in the bottom 400 m of a rocket-triggered lightning channel, *J. Geophys. Res.*, *104*, 14,369–14,376, doi:10.1029/1999JD900201.

Wang, D., N. Takagi, T. Watanabe, V. A. Rakov, M. A. Uman, K. J. Rambob, and M. V. Stapleton (2005), A comparison of channel-base currents and optical signals for rocket-triggered lightning strokes, *Atmos. Res.*, *76*, 412–422.

Wang, D., W. R. Gamerota, M. A. Uman, N. Takagi, J. D. Hill, J. Pilkey, T. Ngin, D. M. Jordan, S. Mallick, and V. A. Rakov (2014), Lightning attachment processes of an anomalous triggered lightning discharge, *J. Geophys. Res. Atmos.*, *119*, 1524–1533, doi:10.1002/2013JD020787.

Xu, Y., and M. Chen (2013), A 3-D self-organized leader propagation model and its engineering approximation for lightning protection analysis, *IEEE Trans. Power Del.*, *28*, 2342–2355.

Zhou, M., D. Wang, J. Wang, N. Takagi, W. Gamerota, M. Uman, D. Jordan, J. Pilkey, and T. Ngin (2014), Correlation between the channel-bottom light intensity and channel-base current of a rocket-triggered lightning flash, *J. Geophys. Res. Atmos.*, *119*, 13,457–13,473, doi:10.1002/2014JD022367.